ACS OMEGA

http://pubs.acs.org/journal/acsodf

Article

Insight into the Process and Mechanism of Water–Rock Interaction in Underground Coal Mine Reservoirs Based on Indoor Static Simulation Experiments

Kai Zhang,* Xu Deng, Ju Gao, Shuyu Liu, Fuyao Wang, and Jinglong Han

Cite This: *ACS Omega* 2022, 7, 36387–36402

Read Online

ACCESS | Metrics & More | Article Recommendations

ABSTRACT: During the storage of underground water reservoirs in coal mines, water–rock interaction occurred between mine water and collapsed rocks, resulting in improved mine water quality, but the water–rock process and mechanism have not been clarified. In this study, six sets of simulated experiments were designed to investigate the water–rock interaction between two types of roof collapse rocks and different water samples in the Daliuta coal mine. The ion ratio method and multivariate statistics are used to reveal the process and mechanism of water–rock interaction during the experimental process from the perspective of input and output water chemical characteristics and rock properties, respectively. The results show that the ion concentration of the effluent water is controlled by water–rock interaction, and the water–rock process mainly involves the dissolution of halite, silicate, pyrite, calcite, dolomite, magnesia chlorite, and gypsum precipitation and is accompanied by ion exchange. Mineral dissolution and precipitation are the most important factors affecting the ion abundance in the effluent. There are differences in the reaction rate, degree of reaction, and dissolution process during the experimental process of fine sandstone and mudstone. Fine sandstone is more reactive than mudstone in terms of reaction rate and degree of reaction, and fine sandstone is dissolved from surface pores to inside and around, while mudstone is generated in new dissolved pores. We found that rock type, ion concentration in the input water, and rock reaction period influence the water–rock interaction during the experiment. The results provide a reference for clarifying the water–rock interaction during the storage of underground water reservoirs in coal mines and predicting the water quality of the effluent.

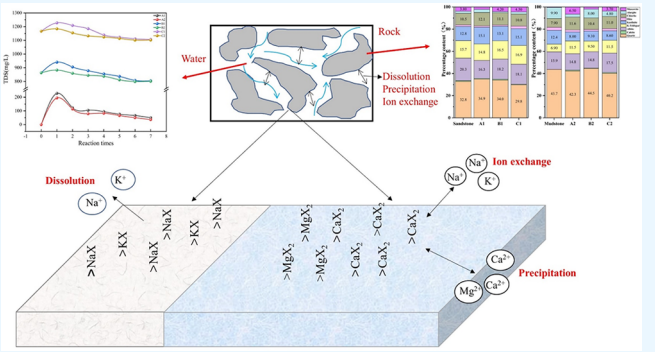

1. INTRODUCTION

Water shortage in western China has severely limited the development of the local coal industry. The operation of the underground water reservoir in the coal mine avoids the loss of mine water and alleviates the water shortage in the arid western region.[1] Daliuta coal mine is the earliest group of underground reservoirs built in China's Shendong mining area. During the operation of the underground reservoir, it was found that the water quality of the mine water was significantly improved after being stored in the reservoir for a period of time. The concentration of suspended matter, calcium ions, COD (chemical oxygen demand), DOM (dissolved organic matter), heavy metals, etc. in mine water is reduced.[1−3] This is due to the surface effect, structure effect, dissolution effect, pore effect, ion exchange effect, and redox effect of natural minerals to purify pollutants.[4] It can be seen that the study of mine water contaminants in underground reservoirs of coal mines is relatively mature. However, there are fewer studies on conventional ions in mine water from coal mine groundwater reservoirs. The concentration of conventional ions affects the subsequent use of mine water.[5] Therefore, it is vital to study the changes in the concentration of major conventional ions in the effluent of coal mine groundwater reservoirs.

The variation of ion concentration in coal mine groundwater reservoir discharge is closely related to water–rock interaction.[6] The water–rock interaction study route can be divided into field investigation and indoor simulation experiments. Field investigation is used to obtain data through field sampling, analyze the data using a series of methods, and speculate on the water–rock interaction process.[7,8] Indoor simulation experiments are often applied to the effects of single factors such as physical sorption, biodegradation, or water–rock interaction on the evolution of groundwater chemical

Received: July 2, 2022
Accepted: September 30, 2022
Published: October 6, 2022

https://doi.org/10.1021/acsomega.2c04161
ACS Omega 2022, 7, 36387–36402

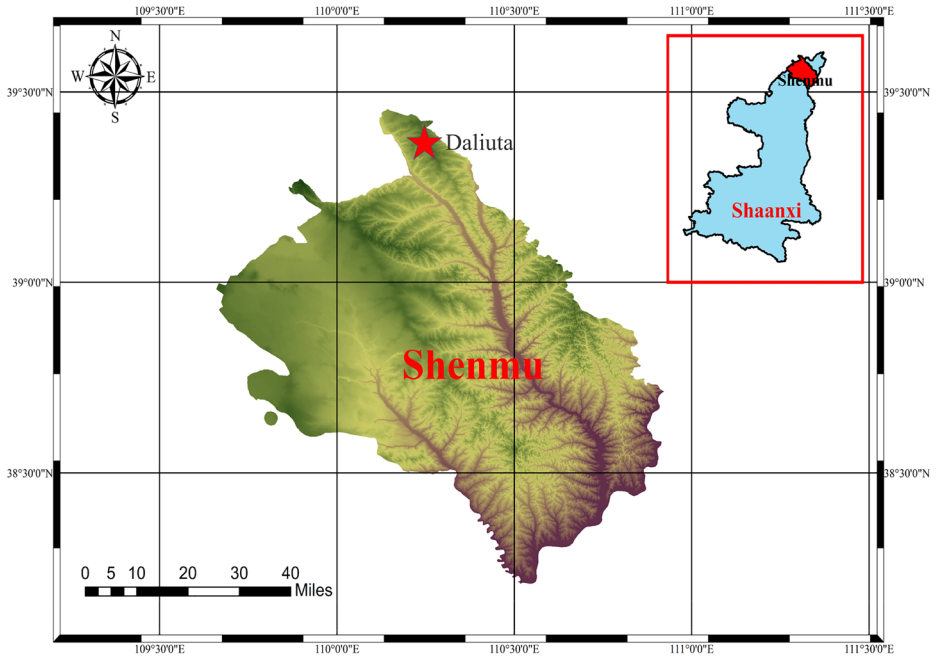

Figure 1. Geographical location of the study area.

fractions.[9] It can approximate the occurrence of water−rock processes such as mineral dissolution, precipitation, and cation adsorption during the evolution of groundwater.[10] And it is also applied to the study of the geochemical characteristics of NGH reservoirs in marine environments.[11] Scholars have studied the water−rock interaction in underground coal mine reservoirs using field investigations and indoor simulations. Zhang[6] analyzed the water−rock interaction process from the perspective of ion change of incoming and outgoing water in coal mines through field investigation and indoor simulation experiments. Fang[7] used SEM and XRD to characterize the microstate of collapsed rocks and found angles and micro-fractures generated during the collapsed rock crushing. And the water−rock simulation experiments proved that these angles and microfissures have apparent adsorption and removal effects on Ca^{2+} and Mg^{2+} in mine water. Although scholars have conducted some research on water−rock interaction in underground reservoirs of coal mines, further research is needed on the ionic changes of water discharge and petrographic changes of the collapsed rocks in underground coal mine reservoirs after multiple water−rock interactions.

At present, scholars mainly obtain data through field investigations and indoor experiments, and use analytical methods of water−rock processes such as multivariate statistics, ion ratio method, and geochemical software simulation to study the water−rock mechanism.[12−15] As a means of data research, geoscientists are now concerned with understanding the geochemical evolution of groundwater using multivariate statistical analysis techniques such as factor analysis and principal component analysis.[16−18] These methods can analyze all parameters and can reduce and classify the data. Even in complex hydrogeological systems, important information can be provided from water chemistry parameters. Ion ratio diagrams are often used in groundwater analysis to resolve the source of ions in water and to infer the dissolution and precipitation processes of minerals from the ratios between major ions.[13,19] In addition, with the continuous development of geosciences, hydrogeochemical simulation software can infer and control the physicochemical processes of groundwater using the major ions in water.[20−22] The most conventional geochemical simulation method in hydro-geochemical studies is the thermodynamically calculated mineral saturation index in PHREEQC. It is able to react to mineral dissolution and precipitation by calculating the saturation index of minerals through water chemistry parameters. Therefore, these methods are widely used in groundwater geochemical evolution, but are not common in resolving water−rock interactions in simulation experiments. Therefore, the combined application of these methods will help to study the water−rock interaction during the simulation experiments.

In this study, the water−rock interaction between fracture water, mine water, deionized water, and two types of roof collapse rocks (fine sandstone and mudstone) in Daliuta coal mine is studied. The design comprises indoor static simulation experiments with different water intake, rock properties, and rock reaction cycles. It includes the analysis of ion concentration changes in water before and after different stages of water−rock interaction, and characterization of rock microscopic changes by scanning electron microscopy (SEM), XRD, XRF, etc. The water−rock interaction processes occurring are analyzed by the integrated ion ratio method, rock characteristic change analysis, and the hydrogeochemical simulation software PHREEQC. The results of the study can predict the sources and migration and transformation patterns of major ions in the effluent of coal mine underground reservoirs at different stages of operation, identify the main factors affecting the ion concentration of the reservoir effluent, and provide a reference and theoretical basis for the comprehensive utilization of mine water in subsequent coal mine underground reservoirs.

2. STUDY AREA

The study area of this paper (Figure 1), Daliuta coal mine, is located in the northwestern area of Shenmu, Yulin City, Shaanxi Province, China. The geographical coordinates of this

https://doi.org/10.1021/acsomega.2c04161
ACS Omega 2022, 7, 36387−36402

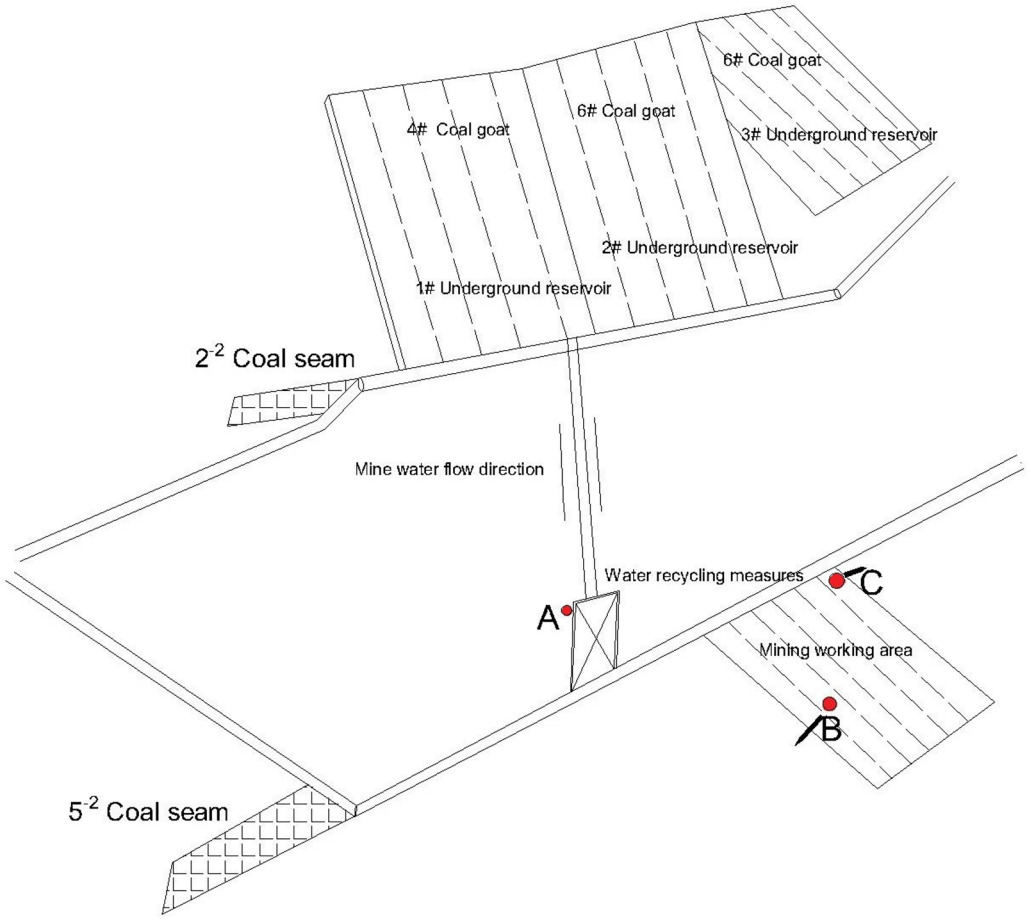

Figure 2. Location of sample collection from underground water reservoirs in coal mines.

well field are 110°12′23″E−110°22′54″E, 39°13′53″N−39°21′32″N. The mine is located in the transition zone from hills, forests, and grasslands to deserts and Gannan grasslands, and belongs to the desert grassland area, close to a semidesert nature, with very little natural vegetation. The climate type is warm temperate arid, semiarid continental monsoon climate, the mine area is dry and hot in summer, cold, dry, and arid in winter, with a long wind and frost period. The annual evaporation is about 2297.4 to 2838.7 mm, and the multiyear average evaporation is about 2111.2 mm, which is 4−5 times that of the rainfall in the area. The average annual rainfall in the mine area ranges from 194.7 to 531.6 mm,[23] and the rainy season is mostly concentrated in July, August, and September each year, accounting for about 67% of the total annual precipitation, mostly in the form of heavy rainfall.

The main aquifers in the well field are the Quaternary valley alluvium diving in the basin of Ulanmulun River and Bronuche River, the Quaternary Upper Pleistocene Salausu Formation diving in the lower part of the terrain in the area, and the sand and gravel layer aquifer of the Lower Pleistocene Sanmen Formation of the Quaternary System, which is distributed above the bedrock in the central part of the well field and below the Lixin loess layer. The layer is in direct contact with the loose sand layer of the Fourth Series locally and the thickness is 0−27.4 m, with an average thickness of 11.77 m, and the thickness of the aquifer is 0.10−27.48 m, with an average value of 8.24 m. The well field also has the Mesozoic clastic fissure aquifer exposed in the area of Haragou, Motherhegou, and Wangquegou.

The coal-bearing strata in the well field are the Middle and Lower Jurassic Yan'an Formation, and the coal resources are characterized by a large number of recoverable coal seams, shallow burial, thin bedrock, and thick overlying loose sand layers, etc.[6] According to the drilling data statistics, the burial depth of 2^{-2} coal seam is 30.6−133.3 m, and the proportion of shallow burial depth and thin bedrock in the distribution area is larger; the burial depth of 5^{-2} coal seam is 162.9−280.0m, which is medium burial depth, and there are 9 recoverable coal seams in the coal seam Yan'an Group, and the main recoverable coal seam is 2 (2^{-2} coal, 5^{-2} coal). The overlying bedrock of the coal seam is mainly composed of siltstone, sandstone, and mudstone, and mostly belongs to the moderate riser-type roof.[24]

3. MATERIALS AND METHODS

3.1. Sample Collection and Pretreatment. Mine water was collected at the 5^{-2} coal seam No. 1 reservoir recycling unit A at the Daliuta coal mine. Fissure-gushing water from the overlying rock seam at point C of the 5^{-2} coal seam comprehensive mining workings was collected. Collapsed rock samples were collected at point B of the coal mining face (Figure 2). The pH and conductivity of water samples were determined on site using a HI98129 multiparameter tester. The water samples were stored in polyethylene containers and immediately transported back to the laboratory for testing of other indicators. The fissure water and mine water collected in the field were passed through a 0.45 μm

https://doi.org/10.1021/acsomega.2c04161
ACS Omega 2022, 7, 36387−36402

Table 1. Water Quality Index of Experimental Water (mg/L)

Sample	pH	EC(μs/cm)	TDS	Na^+	K^+	Ca^{2+}	Mg^{2+}	Cl^-	SO_4^{2-}	HCO_3^-
Mine water	7.36	1960.00	1166.87	338.53	5.81	64.20	15.35	248.67	347.94	292.76
Fracture water	7.96	1267.00	863.29	183.04	3.68	82.36	20.54	217.23	258.32	196.24

Table 2. Chemical Composition of Rock Samples (%)[a]

Component	CO_2	Na_2O	MgO	Al_2O_3	SiO_2	P_2O_5	SO_3	Cl	K_2O	CaO
Fine Sandstone	6.184	1.097	0.864	22.405	59.199	0.184	0.076	0.019	3.935	0.871
Mudstone	8.635	1.035	1.224	19.100	59.614	0.206	0.059	0.014	3.555	0.448
Component	TiO_2	V_2O_5	Cr_2O_3	MnO	Fe_2O_3	Co_2O_3	NiO	CuO	ZnO	Ga_2O_3
Fine Sandstone	0.835	0.023	0.011	0.039	4.168	0.003	0.006	0.003	0.014	0.003
Mudstone	0.893	—	0.013	0.038	5.059	0.002	0.006	0.005	0.026	0.003
Component	As_2O_3	Rb_2O	SrO	Y_2O_3	ZrO_2	Nb_2O_5	Br	CdO		
Fine Sandstone	0.002	0.012	0.014	0.003	0.028	0.002	—	—		
Mudstone	—	0.012	0.017	0.003	0.028	0.003	—	—		

[a]Note: —, Below the test level.

filter membrane to remove suspended matter from the water to prevent interference with the test rock characterization. The filtered water samples were sealed and stored separately. Rock samples were collected using plastic sample bags and characterized for rock phenology and mineral properties. The results show that the rock samples are mainly two types: fine sandstone and mudstone. The collected fine sandstone and mudstone were crushed to a particle size of about 8 mm, followed by washing with deionized water to remove the surface charge and dust impurities generated during the crushing process, and then dried in a constant temperature drying oven and cooled at room temperature.

3.2. Experimental Design and Sample Analysis. The pretreated fine sandstone and mudstone samples of 100 g each were packed into labeled 250 mL corked conical flasks, and 200 mL of deionized water, fissure water, and mine water was added, capped with a plunger, and sealed with a sealing film. After the samples were mixed well, the conical flask was put into a constant temperature water bath oscillator, the temperature was adjusted to 23 °C, and the experiment was carried out at a constant speed of 100 r/min. Before the experiment, we conducted a soaking pre-experiment, and the study found that the EC value in the effluent remained unchanged after 72 h of soaking. Hence, we considered it to be basically in the final stage. Therefore, we designed the soaking experiment for 72 h as one experimental section. After every 72 h, the conical flask was taken out and left for 10 min, and the supernatant in the conical flask was extracted and tested for the concentration of the main anions and cations in the water sample after passing through a 0.45 μm filter membrane, thus completing a static simulation experiment. The remaining rock sample in the conical flask was rinsed several times with deionized water to remove the ions attached to the mineral surface and dried in an oven. The experiment was repeated with the dried rock samples until 7 cycles were completed. After the 7 experiments, the rock samples were removed, washed with deionized water, dried, and ground to pass through a 200 mesh sieve. Characterization of rock mineral variations, pore distribution, and rock surface structure distribution was performed by XRD, SEM, and BET.

In this study, the water quality indicators measured were TDS (total dissolved solids), HCO_3^-, Na^+, K^+, Ca^{2+}, Mg^{2+}, SO_4^{2-}, and Cl^-. TDS was measured in the water samples using the weighing method;[25] HCO_3^- was titrated using a double-mixed indicator; Na^+, K^+, Ca^{2+}, Mg^{2+}, SO_4^{2-}, and Cl^- were determined using a Thermo Scientific Dionex ICS-5000+HPIC high-pressure ion chromatograph.[26] Each indicator was tested 3 times to take the average value, and samples with equilibrium charge greater than 10% were removed. The rock samples were ground to 200 mesh sieve and analyzed for mineralogical composition using a SmartLab SE X-ray diffractometer XRD (Cu target, Kα radiation, step 0.02°, power 40 kV, 150 mA, continuous scanning) manufactured by Rigaku, Japan, with the following test conditions: 2θ angle range of 5−80°, scanning speed setting of 4° /min. A Phenom scanning electron microscope was used to analyze the surface morphology of the rock samples before and after the reaction, and the corresponding magnification was set according to the effect obtained from the field observation. The ASAP 2020 M rapid specific surface/pore analyzer was used to determine and analyze the specific surface area and total pore volume/average pore size of rock samples. The measurement range of specific surface area of the instrument was set to 0.005m^2/g~infinity, the measurement range of pore size distribution was set to 0.35−500 nm, and the minimum detection limit of pore volume analysis was 0.0001 cm^3/g (by H−K or DA analysis).

3.3. Data Analysis Methods. PCA is the main statistical technique used in this study, which can be used to reduce the complexity of large-scale data sets and to show the relationship between data components by considering a factor with an eigenvalue ≥1 as a possible variable. In this study, SPSS software 26.0 was used for multivariate statistical analysis. The extraction factor method was PCA, and the rotation criterion was the maximum variance method.

Equation 1 is thermodynamic calculation with the use of PHREEQC of the saturation index (SI) of various mineral phases in water.[13]

$$\mathrm{SI} = \log \frac{\mathrm{IAP}}{K_s(T)} \tag{1}$$

where IAP is the ionic activity of the solution and $K_s(T)$ is the solubility constant at a specific temperature. In practice the SI can be considered as quasi-equilibrium when it is between −0.5 and +0.5. If it is less than −0.5, the mineral is considered to be in an unsaturated state and in a dissolved state; conversely, if it is greater than +0.5, the mineral is considered to be in a supersaturated state and in a precipitated state.

https://doi.org/10.1021/acsomega.2c04161
ACS Omega 2022, 7, 36387−36402

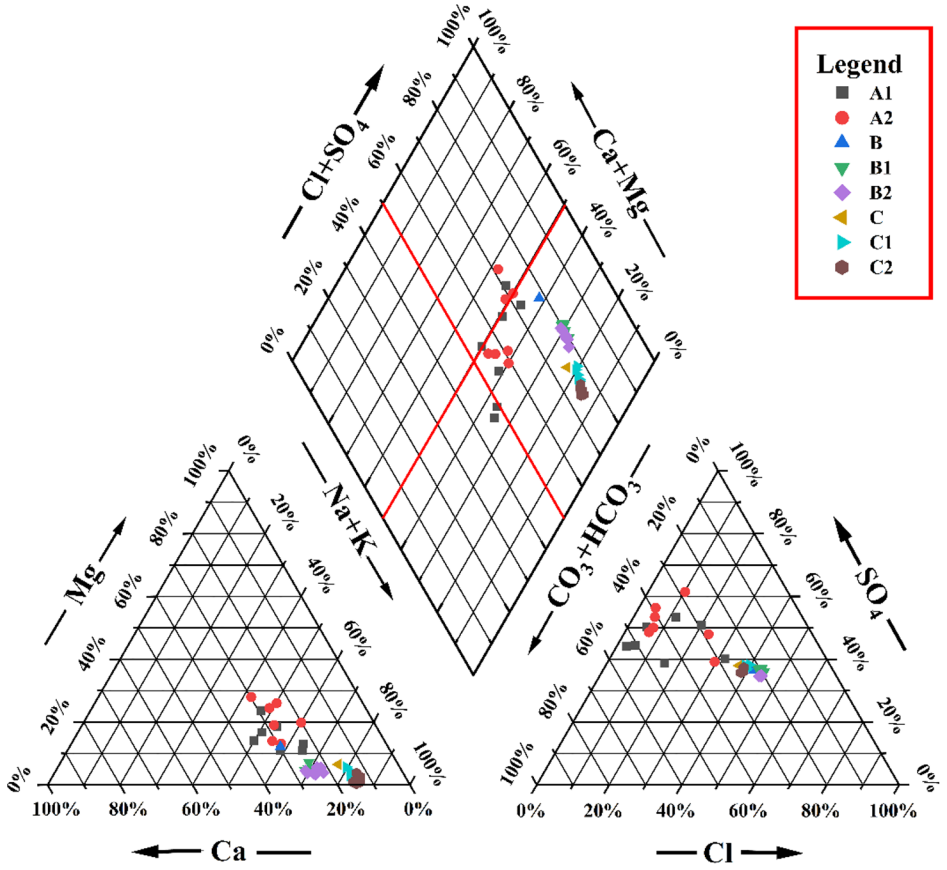

Figure 3. Water sample piper diagram: A1, deionized water−fine sandstone group; A2, deionized water−mudstone group; B, fissure water; B1, fissure water−fine sandstone group; B2, fissure water−mudstone group; C, mine water; C1, mine water−fine sandstone group; C2, mine water−mudstone group.

The Software Platform used was Jade 6.0(MDI, Livermore, CA, USA); data were processed with Excel 2019 software, and graphing was done with Origin 2021 software.

4. RESULTS

4.1. Input Water Quality and Rock Sample Composition. Water quality tests were conducted on mine water and fissure water, and the results are shown in Table 1. The TDS of mine water is 1166.87 mg/L, which is brackish water; the TDS of fissure water is 863.29 mg/L, which is fresh water. The order of ion concentration in mine water is $SO_4^{2-} > Na^+ > HCO_3^- > Cl^- > Ca^{2+} > Mg^{2+} > K^+$. The order of ions in the fissure water is $SO_4^{2-} > Cl^- > HCO_3^- > Na^+ > Ca^{2+} > Mg^{2+} > K^+$. The concentrations of Na^+, Cl^-, SO_4^{2-}, and HCO_3^- in mine water are higher than those in fissure water. However, the concentration of Ca^{2+} and Mg^{2+} in mine water is lower than that of Ca^{2+} and Mg^{2+} in fracture water, and the difference in K^+ concentration is not significant.

The collected rock samples were analyzed by XRF detection, and the results of the spectral semiquantitative mineral element composition analysis are shown in Table 2. The main components of both rock samples are SiO_2 and Al_2O_3, and the percentages of oxides of the two elements in fine sandstone and mudstone are 81.604% and 78.714%, respectively. And elements such as K, Na, Ca, Mg, C, Fe, Mn, Ti, S, Cl, etc.

The overall chemical composition of the two rock samples is very similar, but the content of each element differs from each other. The CO_2, Fe_2O_3, and MgO contents of the mudstone are higher than those of the fine sandstone, while the K_2O and Al_2O_3 contents are lower than those of the fine sandstone. According to the results of XRF analysis, the main minerals of the collected rock samples are meta-aluminates and silicates, and there are some common coal seam co-occurring minerals such as gypsum, halite, and pyrite.[27]

4.2. Water Chemistry Characteristics. *4.2.1. Input and Output Water Chemistry Type.* According to the molar concentration of major anions and cations and ionic valence product percentage, a triangular diamond water quality diagram can be constructed. The percentages of major anions and cations of mine water, fissure water, and six groups of experimental effluent water were projected onto a rhombus to draw a piper trilinear diagram, as shown in Figure 3. The water chemistry type of the water samples can be directly reflected according to the difference of the sample points to the distribution area of the rhombus. The experimental input and output water chemistry types were classified using the Shukarev method, and the results showed that most of the output water chemistry types of A1 and A2 groups were the 18-A SO_4Cl-HCO_3Na-Ca type. The water chemistry of fissure water is the 39-A Cl-SO_4-Na-Ca type which is consistent with the water chemistry of Triassic and Jurassic bedrock fissure aquifers in the area west of Shenmu County.[6] The water chemistry type of B1 and B2 effluent gradually changed to 42-A Cl-SO_4-Na. The water chemistry type of mine water is 21-A Cl-SO_4-HCO_3-Na. The water chemistry type of C1 and C2 discharge water is 42-A Cl-SO_4-Na, and the experimental simulated discharge water is in line with the 42-A Cl-SO_4-Na

https://doi.org/10.1021/acsomega.2c04161
ACS Omega 2022, 7, 36387−36402

type water chemistry of Daliuta coal mine groundwater reservoir discharge water.

4.2.2. Variation of Input and Output Water Ion Concentration. The experimental input and output water anion and cation concentrations were analyzed, and the results are shown in Figures 4 and 5. The variation of TDS in the

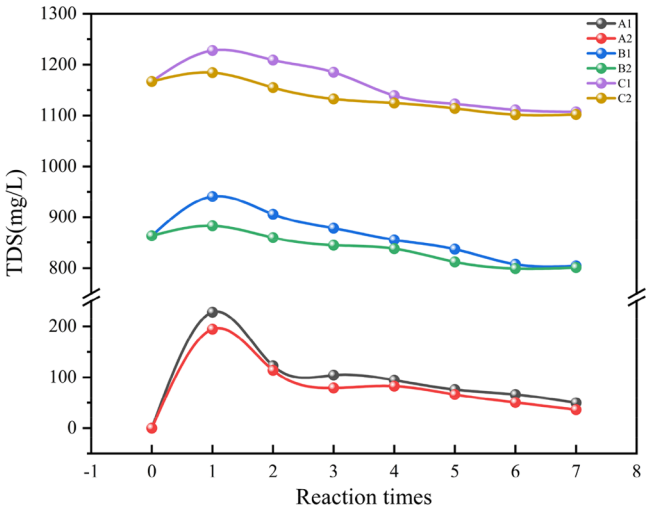

Figure 4. Variation of TDS with rock−water−rock reaction time.

effluent of the two rock samples at different concentrations and cycles (Figure 4). Both rock samples were soaked with deionized water, fissure water, and mine water for many times over a long period of time, and the TDS in the output water showed a trend of first increasing and then decreasing, and finally approached the TDS value of the input water. The first water−rock reaction was the most violent, with the most elevated TDS in the effluent, 228.00 mg/L, 77.40 mg/L, and 60.91 mg/L, respectively. There are differences in the degree of response of the rock samples under different inlet water abundance, from strong to weak, in the order of deionized water, fissure water, and mine water. During the entire experiment, the TDS concentration of the fine sandstone after immersion was always higher than that of the mudstone, indicating that the fine sandstone has a higher content of soluble minerals and is more susceptible to water−rock interaction.

The concentration of each major anion and cation in the output water was changed after the two rock samples were soaked in deionized water several times. The relationship between the magnitude of cation concentration in A1 is $Na^+ > Ca^{2+} > K^+ > Mg^{2+}$, while the relationship between the magnitude of cation concentration in A2 is $Na^+ > Ca^{2+} > Mg^{2+} > K^+$ (Figure 5a,b). It shows that the content of Na-containing soluble minerals in fine sandstone and mudstone is easier to dissolve. The K^+ mass concentration in water after immersion of fine sandstone was higher than that of Mg^{2+}, while the K^+ and Mg^{2+} mass concentrations in water after immersion of mudstone were close. According to the analysis of mineral composition, the low content of the K element and high content of Mg element in mudstone caused the difference of ion concentration in water. After the samples were soaked in deionized water, the mass concentrations of Na^+, K^+, and Ca^{2+} were higher in A1 output water than in A2 output water. The results indicate that the fine sandstone has a high content of soluble cationic minerals or is more soluble, and this result is consistent with the TDS findings (Figure 4). The relationship between the size of the concentration of each ion, A1 and A2 anions, in the output water is $SO_4^{2-} > HCO_3^- > Cl^-$, and then presented as $HCO_3^- > SO_4^{2-} > Cl^-$. This indicates that as the soaking period increases, the sulfur-bearing minerals in the rock decrease, dissolution decreases, and carbonate or silicate dissolution plays a major role.

The concentration of each anion and cation in the output water changed after the two rock samples were soaked by fissure water and mine water several times (Figure 5c−f). The Na^+ and K^+ in the effluent of B1, B2, C1, and C2 all showed a trend of increasing and then decreasing, but the final ion mass concentration was higher than that of the raw water. Ca^{2+} and Mg^{2+} in the effluent of B1, B2, C1, and C2 showed a decreasing trend, and the ion mass concentration was lower than that of the raw water. The Cl^- in B1, B2, C1, and C2 effluent showed a rising and then decreasing trend, and the final ion mass concentration was close to that of the original water. The above results indicate that the dissolution capacity of halite in minerals gradually decreases with the increase of the soaking period and finally reaches the equilibrium state. The trends of HCO_3^- and SO_4^{2-} in the effluent of B1 and C1 are the same, and the trends of HCO_3^- and SO_4^{2-} in the effluent of B2 and C2 are the same. It shows that the water−rock reaction process occurs consistently in the same rocks at different input water abundance. As the reaction period increases, the mass concentration of each anion and cation in the fine sandstone and mudstone effluent shows a gradual decrease, with the largest difference in anion and cation mass concentrations between the first and the second time. It indicates that the first water−rock action has the most intense reaction, which is the same as the change of TDS (Figure 4).

In summary, from the perspective of incoming water ion abundance, the order of rock reaction degree is deionized water group > fissure water group > mine water group. From the perspective of rock sample type, the order of rock reaction degree is fine sandstone > mudstone, and from the perspective of reaction period, the rock reaction degree gradually decreases with increasing period, and the first reaction is the most violent.

4.3. Rock Sample Characteristics. *4.3.1. Rock Sample Composition.* The rock mineral composition was analyzed qualitatively and semiquantitatively before and after the fine sandstone and mudstone experiments using XRD (Figure 6). The percent contents of calcite, sodium feldspar, potassium feldspar and illite, plagioclase, and muscovite were reduced after the fine sandstone was dissolved by deionized water. In contrast, quartz and kaolinite, oolitic chlorite, magnesian chlorite, and manganese mica content are relatively higher. Of these, sodium feldspar and potassium feldspar decreased by 4% and 0.9%, respectively, and kaolinite increased by 2.3%. This indicates that dissolution of sodium feldspar and potassium feldspar occurred mainly in the fine sandstone, and kaolinite was produced. The sodium feldspar, illite and manganese mica contents in the fine sandstone-fissure water test group were reduced by 2.1%, 0.3%, and 0.9%, respectively. Quartz, potassium feldspar, kaolinite, chlorite and muscovite contents increased by 1.1%, 0.8%, 0.3%, 0.6%, and 0.4%, respectively. Calcite content was kept constant. The quartz, calcite, and sodium feldspar contents in the fine sandstone−mine water test group were reduced by 3.1%, 0.3%, and 2.2%, respectively. Potassium feldspar, kaolinite, illite, chlorite, and muscovite contents increased by 1.2%, 2.3%, 1.0%, 0.3%, and 0.7%,

https://doi.org/10.1021/acsomega.2c04161
ACS Omega 2022, 7, 36387−36402

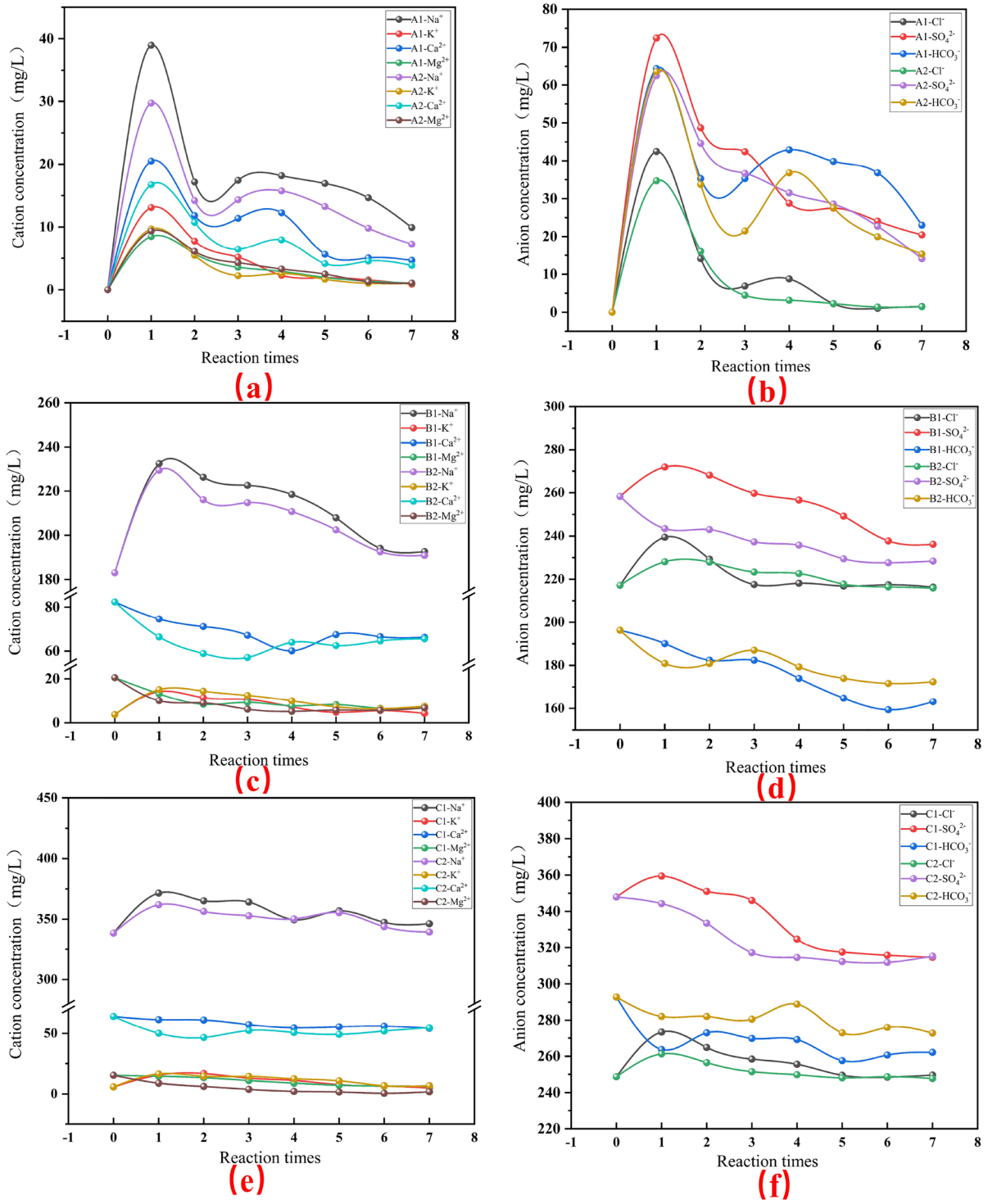

Figure 5. Variation of each anion and cation concentration with the cycle of water−rock interaction: (a,b) fine sandstone and mudstone with deionized water, (c,d) fine sandstone and mudstone with fracture water, (e,f) fine sandstone and mudstone with mine water.

respectively. There are large differences in the changes of mineral content of fine sandstone after immersion in deionized water, fissure water, and mine water, respectively, indicating that the initial ion concentration in water has a large influence on the process of water−rock interaction (Figure 6).

The percentage content of sodium feldspar, quartz and kaolinite, illite, oolitic chlorite, and manganese mica decreases after the mudstone is dissolved by deionized water. While calcite, potassium feldspar and plagioclase, magnesia chlorite, and muscovite content increased. Sodium feldspar, kaolinite, illite, and manganese mica decreased by 1.1%, 4.4%, 0.9%, and 7.3%, respectively. While potassium feldspar and white mica increased by 4.6% and 6.0%, respectively. This shows that when the mudstone is mainly dissolved by manganese mica, potassium feldspar and white mica are produced. Also this process consumed a certain amount of kaolinite. Na-feldspar and illite also underwent dissolution. The sodic feldspar, kaolinite, illite, and manganese mica contents in the mud-

https://doi.org/10.1021/acsomega.2c04161
ACS Omega 2022, 7, 36387−36402

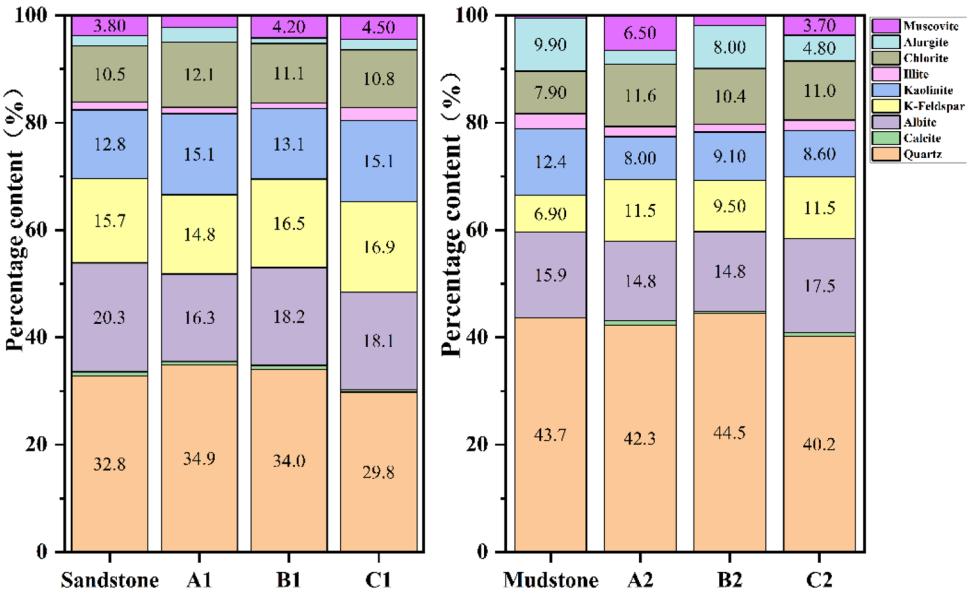

Figure 6. Variation of rock components: A, deionized water; B, fracture water; C, mine water; below 3% not shown.

stone−fissure water group were reduced by 1.1%, 3.3%, 1.4%, and 1.9%, respectively. Quartz, calcite, potassium feldspar, chlorite, and muscovite contents were elevated by 0.8%, 0.4%, 2.6%, 2.5%, and 1.4%, respectively. The quartz, kaolinite, illite, and manganese mica in the mudstone-mine water group were reduced by 3.5%, 3.8%, 0.8%, and 5.1%, respectively. Calcite, sodium feldspar, potassium feldspar, chlorite, and muscovite contents increased by 0.7%, 1.6%, 4.6%, 3.1%, and 3.2%, respectively. It can be seen that there are large differences in the mineral content changes of the mudstone after reacting with different abundances of feedwater. After experiment, there are differences in dissolution and precipitation of mudstone and fine sandstone minerals. The mudstone has less dissolved sodium feldspar and more dissolved manganese mica; however, the fine sandstone has more dissolved sodium feldspar and less dissolved manganese mica. The increase of mudstone chlorite is larger than that of fine sandstone, indicating that the mudstone has a stronger ability to adsorb Mg^{2+} in water, which is beneficial to reduce the hardness of the effluent water.

4.3.2. Pore Structure of Rock Samples. From Figure 4 and Figure 5, it can be seen that the two rock samples reacted more violently under deionized water immersion; therefore, in this study, BET tests were performed on the two rock samples after deionized water immersion to analyze the changes in their pore structures (Table 3−5). The specific surface area of fine sandstone increased from the average value of 6.18 m^2/g before the reaction to 6.44 m^2/g. The average value of specific surface area of mudstone before reaction was 8.65 m^2/g, which increased to an average value of 9.14 m^2/g after the reaction (Table 3).

The total pore volume of fine sandstone and mudstone changed, and the total pore volume of fine sandstone increased from the average value of 0.0218 cc/g before dissolution to 0.0236 cc/g, and the total pore volume of mudstone increased from the average value of 0.0269 cc/g before dissolution to 0.0273 cc/g (Table 4). The reaction of fine sandstone and mudstone with deionized water increased the specific surface area and total pore volume of the rocks. This indicates that the surface minerals of fine sandstone and mudstone have been dissolved and the surface dissolution pore space has increased.

The mean pore size of fine sandstone increased from 13.47 to 13.95 nm, while the mean pore size of mudstone decreased from 11.89 to 11.42 nm before and after the simulation experiment (Table 5).

Author: The average pore size of fine sandstone increases, while the average pore size of mudstone decreases. It shows that the dissolution mechanism of fine sandstone and mudstone is different, and the fine sandstone may be the result of a dissolution reaction to the interior or periphery on the basis of the original pores, while the mudstone may have a mechanism of a hole collapse to produce more fine pores.

Table 3. Analysis of the Rock Specific Surface Area before and after Water Karst Exhalation (m^2/g)

Sample[a]	BET	Langmuir	BJH Adsorption accumulation of specific surface area	BJH Desorption accumulated specific surface area
Fine Sandstone	5.75	7.19	5.51	6.26
Fine sandstone-1	6.05	7.57	5.65	6.49
Mudstone	8.30	9.73	7.73	8.86
Mudstone-1	8.79	10.32	8.13	9.32

[a]Note: 1 represents the sample after reaction.

Table 4. Analysis of Total Pore Volume of the Rock before and after Water Karstification (cc/g)

Sample[a]	Total pore volume for single point adsorption	BJH Total pore volume of adsorption accumulation	BJH Desorption cumulative total pore volume
Fine Sandstone	0.0219	0.0216	0.0219
Fine Sandstone-1	0.0237	0.0233	0.0237
Mudstone	0.0271	0.0265	0.0270
Mudstone-1	0.0275	0.0269	0.0274

[a]Note: 1 represents the sample after reaction.

https://doi.org/10.1021/acsomega.2c04161
ACS Omega 2022, 7, 36387−36402

Table 5. Analysis of Rock Pore Size before and after Water Karst Exhalation (nm)

Sample[a]	Adsorption average pore size	Desorption average pore size	BJH adsorption average pore size	BJH desorption average pore size
Fine Sandstone	15.22	9.04	15.64	13.99
Fine Sandstone-1	15.69	9.03	16.51	14.59
Mudstone	13.08	8.61	13.73	12.17
Mudstone-1	12.52	8.19	13.23	11.76

[a]Note: 1 represents the sample after reaction.

4.3.3. Rock Sample Surface Morphology. To further characterize the rock surface shape, SEM scanning electron microscopy was used to observe the surface morphology of both rock samples (Figure 7). The fine sandstone was soaked with deionized water to increase the dissolution pores, and the distribution between the particles was more dispersed (Figure 7a,b). The cemented material on the surface of fine sandstone is gradually dissolved and corroded, and the fracture development inside the rock is more obvious. A large number of dissolution pores appear on the surface, and the accumulation structure between mineral particles is gradually destroyed.

The mudstone was gradually eroded on the surface and its original angular and microfracture edges inside by deionized water immersion, and the original lamellar kaolinite structure in the rock minerals had a tendency to change to agglomerate structure, and the superficial kaolinite gradually decreased (Figure 7c,d). And the sparseness between the rock structures increases, the pores formed by dissolution increase, and the pore development inside the rock gradually increases, which is consistent with the results of pore structure analysis. The larger pore structure makes it easier for the mudstone to adsorb ions in water, and the ion concentration in the effluent is lower.

4.4. Multivariate Statistical Analysis. Principal component analysis (PCA) is a statistical method used to decompose multiple variables into several complete, uncorrelated variables while retaining the most original data information. It is widely used for groundwater−water chemical characterization.[28] Multivariate statistical techniques applied to water chemistry data can show their interrelationships and thus help decipher their origin.[29]

In this study, there was only one principal component extracted during the principal component analysis of the 14 experimental samples of the deionized water group, which could explain 92.52% of the sample variance, which could represent the dissolution of the minerals. A total of 28 experimental samples from the fracture water and mine water groups were analyzed by PCA to decompose variables such as Na^+, K^+, Ca^{2+}, Mg^{2+}, Cl^-, SO_4^{2-}, HCO_3^-, and TDS. The correlation analysis between the ions (Table 6) showed a significant positive correlation between TDS and Na^+, K^+, Cl^-, SO_4^{2-}, and HCO_3^- and a significant negative correlation with Ca^{2+} ($r = -0.685$).

Since the raw data showed a nonpositive distribution, the data were normalized and standardized using the SPSS 26.0 software package before PCA analysis was performed. The calculated KMO was 0.712, the factor analysis was good, and Bartlett's sphericity test was met. The PCA results showed that a total of two principal components were selected, and their total variance contribution exceeded 91% (Table 7). Na^+, Ca^{2+}, Cl^-, SO_4^{2-}, HCO_3^-, and TDS had high loading values in the

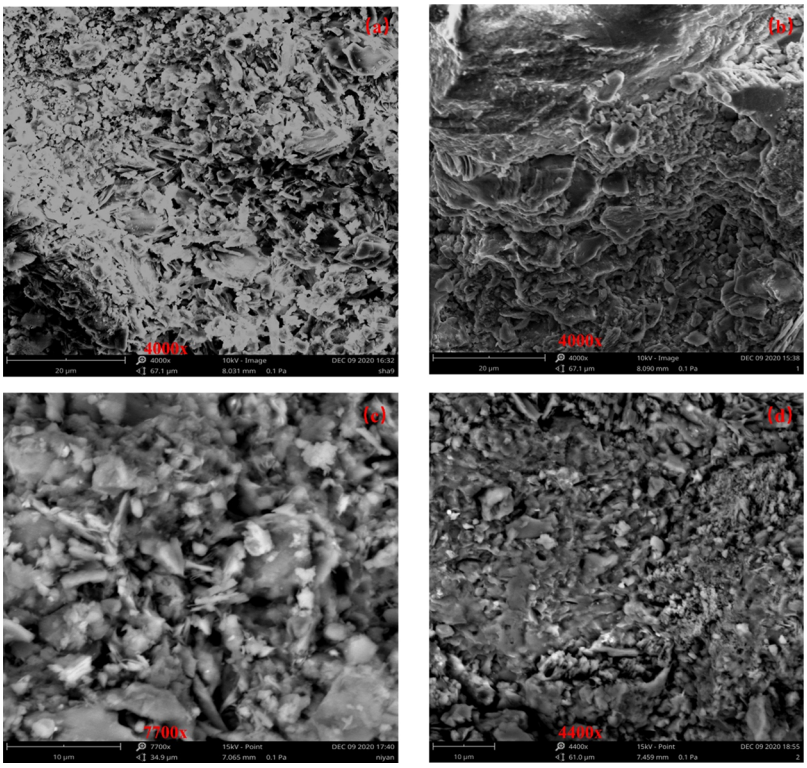

Figure 7. Scanning electron microscope morphology before and after water−rock interaction: (a) Fine sandstone before the reaction, (b) fine sandstone after reaction, (c) mudstone before the reaction, (d) mudstone after reaction.

https://doi.org/10.1021/acsomega.2c04161
ACS Omega 2022, 7, 36387−36402

Table 6. Correlation Matrix of Factor Analysis on Major Ions from 28 Water Samples[a]

	Na^+	K^+	Ca^{2+}	Mg^{2+}	Cl^-	SO_4^{2-}	HCO_3^-	TDS
Na^+	1.000	0.361	−0.753**	−0.060	0.955**	0.971**	0.984**	0.991**
K^+		1.000	−0.169	0.468*	0.529**	0.432*	0.361	0.440*
Ca^{2+}			1.000	0.500**	−0.615**	−0.634**	−0.809**	−0.685**
Mg^{2+}				1.000	0.161	0.123	−0.178	0.054
Cl^-					1.000	0.973**	0.927**	0.981**
SO_4^{2-}						1.000	0.938**	0.991**
HCO_3^-							1.000	0.968**
TDS								1.000

[a]Note: **$p < 0.01$, *$p < 0.05$.

PC1 direction, with PC1 explaining 69.524% of the sample variance (Table 6).

Table 7. Rotation Matrix Extracted Using Principal Component Analysis (Bold Values Indicate Good Positive Loadings for Each Factor)

Parameter	PC 1	PC 2
Na^+	**0.990**	0.049
K^+	0.394	**0.703**
Ca^{2+}	**-0.818**	0.416
Mg^{2+}	−0.129	**0.944**
Cl^-	**0.943**	0.291
SO_4^{2-}	**0.953**	0.224
HCO_3^-	**0.994**	−0.042
TDS	**0.977**	0.171
Total initial eigenvalue	5.562	1.727
Percentage of variance	69.524	21.592
Cumulative % of variance	69.524	91.116

Na^+, Cl^-, SO_4^{2-}, HCO_3^-, and TDS showed positive loadings on PC1, while Ca^{2+} showed negative loadings (Figure 8). PC1 may dissolve with minerals in the water−rock interaction (rock salt, pyrite, etc.), releasing ions from the minerals into the water and causing an increase in the ion concentration in the water. PC2 explained 21.592% of the sample variance, and Mg^{2+} and K^+ had high positive loading values in the PC2 direction (Figure 8). PC2 may be related to the ion exchange between K−Mg, resulting in a lower Mg^{2+} concentration in the effluent.

5. DISCUSSION

5.1. Water−Rock Interaction Process. To further understand the water−rock interaction process in the experiment, the ion ratio method was used to explain the main ion sources in water. According to the binary diagram, the Na^+/HCO_3^- over Na^+/Ca^{2+} ratio, and the Na^+/Mg^{2+} over Na^+/Ca^{2+} ratio can determine the type of mineral dissolution.[30,31] In this study, Na^+/HCO_3^- over Na^+/Ca^{2+} and Na^+/Mg^{2+} over Na^+/Ca^{2+} binary plots were plotted based on the ion concentrations of the six groups of experimental effluent water (Figure 9).

Group A1 and A2 are all located in the silicate zone, indicating that the ions in the effluent of the deionized group

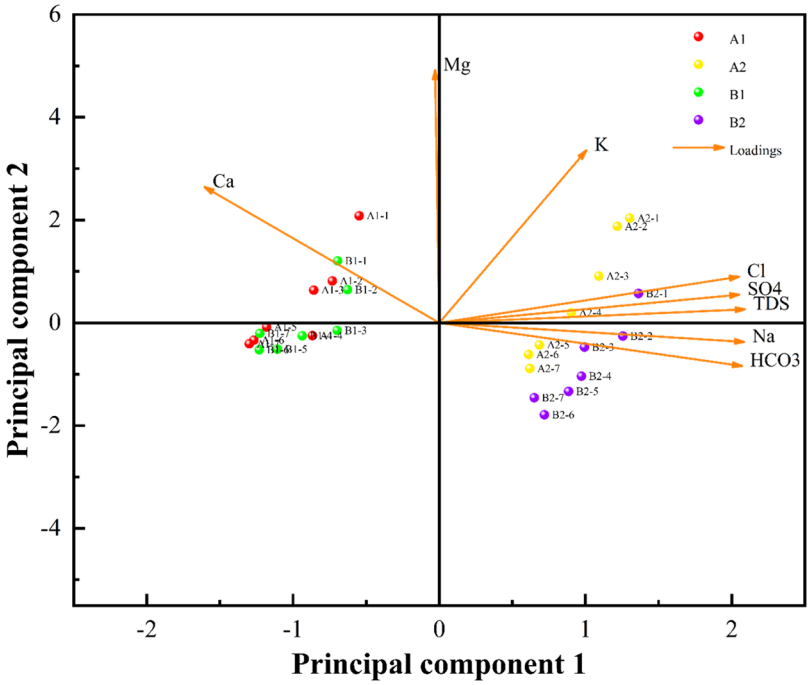

Figure 8. Biplot from the PCA for water samples: A1, fine sandstone−fissure water; A2, fine sandstone−mine water; B1, mudstone−fissure water; B2, mudstone−mine water.

https://doi.org/10.1021/acsomega.2c04161
ACS Omega 2022, 7, 36387−36402

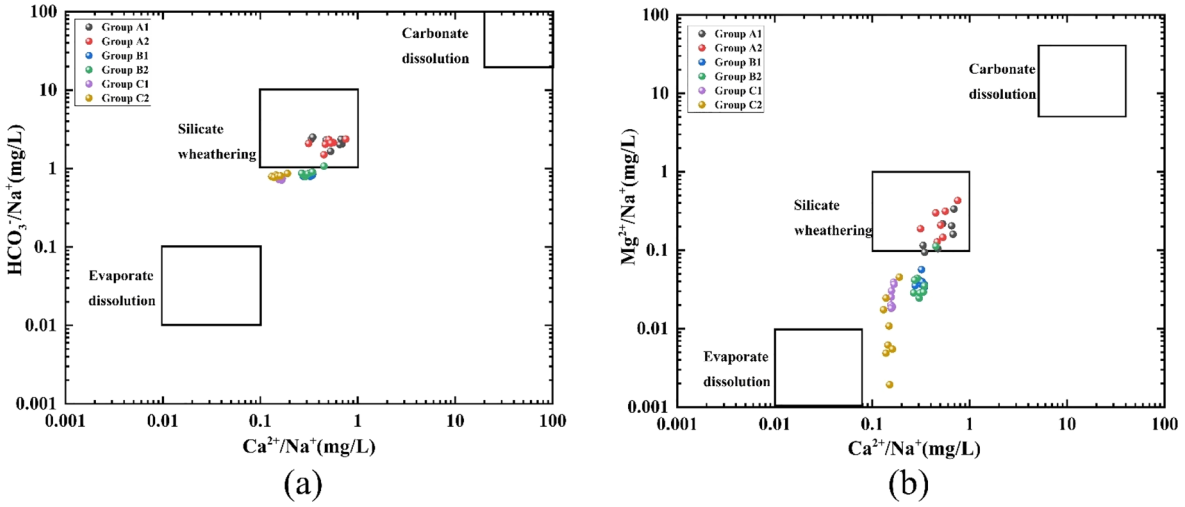

Figure 9. Bivariate plot of (a) Na^+/HCO_3^- over Na^+/Ca^{2+}, (b) Na^+/Mg^{2+} over Na^+/Ca^{2+}.

are mainly derived from the dissolution of silicate minerals. Groups B1, B2, C1, and C2 are located between the silicate zone and the evaporative dissolution zone, indicating that the ions in the water mainly originate from the dissolution of Silicate and Evaporative minerals. The ion sources in water are basically the same for both fine sandstone and mudstone rocks under the same water sample conditions, indicating that the mineral dissolution processes are similar for both rock samples.

The binary diagram of major ions (Na^+, K^+, Ca^{2+}, Mg^{2+}, HCO_3^-, SO_4^{2-}) versus Cl^- can illustrate the possible sources of major elements.[32] The Na/Cl ratio is an important factor in determining the source of Na^+ and Cl^-. If these ions are from halite dissolution, the ratio should be unity, and if the ratio deviates from unity, it indicates that Na^+ and Cl^- have other sources.[33] All experimental water samples were located above the halite dissolution line with a high correlation between Na^+ and Cl^- ($r = 0.946$) (Figure 10a). The Na^+ to Cl^- ratio in the effluent of the deionized water group is close to 1:1, indicating that the Na^+ and Cl^- in the effluent mainly originate from the dissolution of halite. However, Na^+ is enriched relative to Cl^- in the effluent of the fissure and mine water groups, which indicates that Na^+ is not only derived from the dissolution of halite, but also from other processes such as the dissolution of silicate minerals.

The concentration of K^+ was relatively low in all water samples, and a similar trend of variation between K^+ and Cl^- in the deionized water group indicates that the K^+ in the effluent may originate from KCl dissolution. However, the trend of K^+ and Cl^- changes in the fissure water and mine water groups are not obvious and may be controlled by other processes. As shown in Figure 9, dissolution of sodium-silicate minerals such as sodium feldspar, manganese mica, or white mica, and potassium-containing minerals occurred in the fine sandstone and mudstone in the mine water and fissure water groups. The main reaction in which sodium feldspar can be dissolved at 25 °C and atmospheric pressure is given as eq 2.[34]

$$2NaAlSi_3O_8 + 2H_2CO_3 + 9H_2O \rightarrow H_4Al_2Si_2O_9 + 2Na^+ + 2HCO_3^- + 4H_4SiO_4 \quad (2)$$

Na^+ and K^+ can also be generated by the dissolution of manganese mica and white mica in the rocks, and white mica may also be generated during the dissolution of manganese mica (eq 3) (eq 4), which makes the white mica in the rocks increase.

$$(K_{0.94}Na_{0.06})(Mg_{0.08}Al_{1.75}Fe_{0.15}Mn_{0.02})(Al_{0.92}Si_{3.08})O_{10}(OH)_2 + H^+ + H_2O \rightarrow H_4Al_2Si_2O_9 + K^+ + Na^+ + Mn^{2+} + Fe^{3+} \quad (3)$$

$$(K_{0.82}Na_{0.18})(Fe_{0.03}Al_{1.97})(AlSi_3)O_{10}(OH)_2 + H^+ + H_2O \rightarrow H_4Al_2Si_2O_9 + K^+ + Na^+ + Fe^{3+} \quad (4)$$

K^+ in water may also originate from the dissolution of potassium feldspar and illite as in eq 5 and eq 6.[35]

$$2KAlSi_3O_8 + 2H^+ + H_2O \rightarrow H_4Al_2Si_2O_9 + 2K^+ + 4SiO_2(\text{siliceous}) \quad (5)$$

$$(K, H_3O)Al_2Si_3AlO_{10}(OH)_2 + H^+ + H_2O \rightarrow H_4Al_2Si_2O_9 + 2K^+ \quad (6)$$

The Ca−Cl, SO_4−Cl, and HCO_3−Cl relationship plots show a typical increase in Ca^{2+}, SO_4^{2-}, and HCO_3^- with increasing Cl^-, reflecting a possible progressive reaction of halite with carbonate and evaporite (Figure 10c,e,f). A plot of the Mg−Cl relationship shows the distribution of Mg^{2+} along the 1:1 line in the deionized water group. However, there is no regular distribution of Mg^{2+} in fissure water and the mine water group, This indicates that Mg^{2+} in water is controlled by other water chemistry, such as dolomite and magnesia chlorite precipitation.

If Ca^{2+}, Mg^{2+}, SO_4^{2-}, and HCO_3^- originate only from the dissolution of carbonate such as calcite, dolomite (eq 7, eq 8, eq 9) and evaporated minerals (e.g., gypsum, hard gypsum, etc.), the ratio of $(Ca^{2+}+Mg^{2+})/HCO_3^-$ mg-equivalent concentration should be 1 based on the chemical composition of carbonate and the evaporated minerals.[32]

If calcite dissolves

$$CaCO_3 + H_2CO_3 \rightarrow Ca^{2+} + 2HCO_3^- \quad (7)$$

the congruent dolomite dissolution is

https://doi.org/10.1021/acsomega.2c04161
ACS Omega 2022, 7, 36387−36402

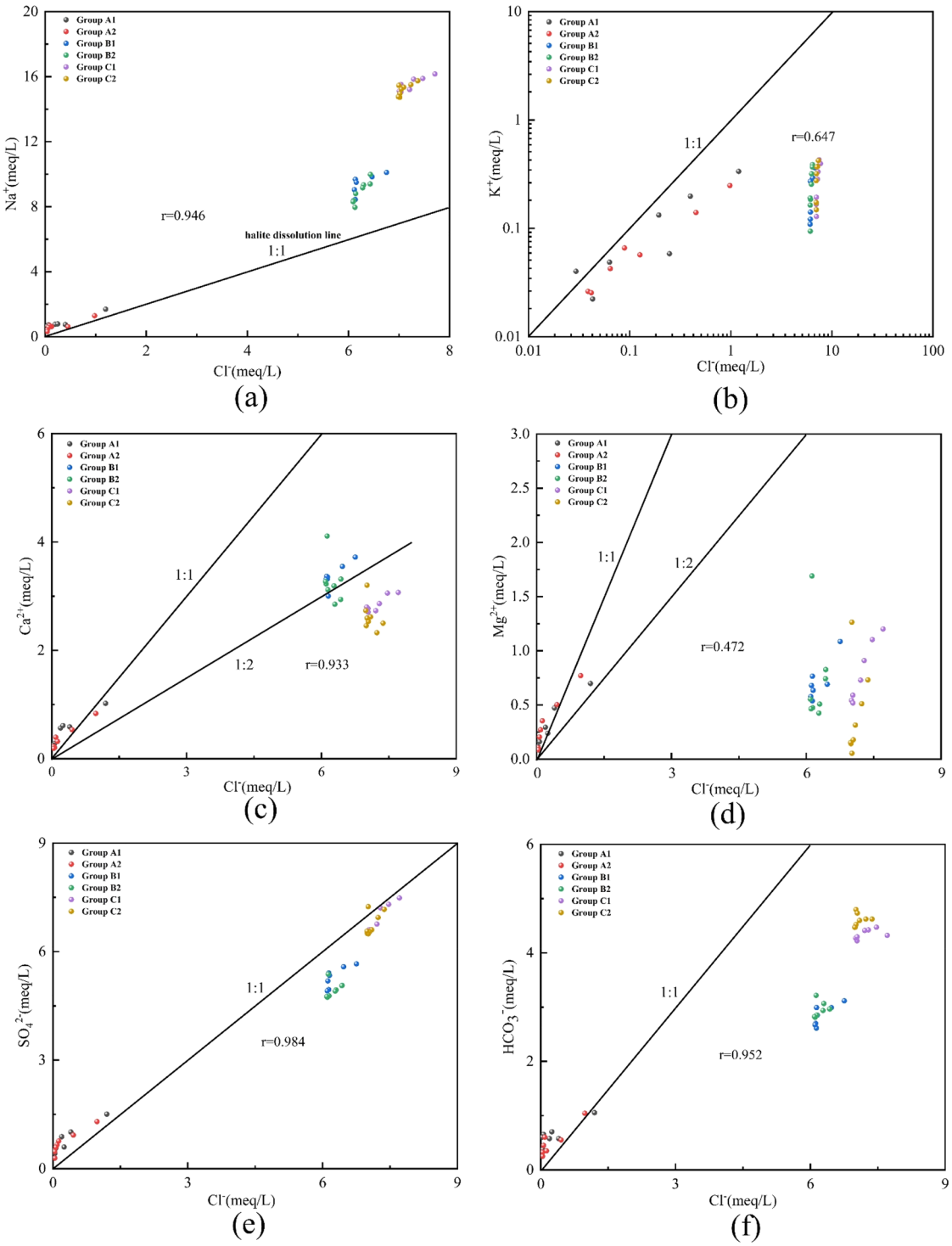

Figure 10. Relationship between major ions and chlorine, showing possible sources of major elements: (a) Na^+ vs Cl^-, (b) K^+ vs Cl^-, (c) Ca^{2+} vs Cl^-, (d) Mg^{2+} vs Cl^-, (e) SO_4^{2-} vs Cl^-, (f) HCO_3^- vs Cl^-.

$$CaMg(CO_3)_2 + 2H_2CO_3 \rightarrow Ca^{2+} + Mg^{2+} + 4HCO_3^- \quad (8)$$

and the incongruent dolomite dissolution is

$$CaMg(CO_3)_2 + H_2CO_3 \rightarrow CaCO_3 + Mg^{2+} + 2HCO_3^- \quad (9)$$

All samples of the deionized water group were distributed near the dissolution line. All samples of the fissure water group were located above the dissolution line. All samples of the mine water group were located below the dissolution line (Figure 11a). It shows that Ca^{2+} and Mg^{2+} of both rocks under deionized water conditions are mainly derived from carbonate. Under fractured water conditions, Ca^{2+} and Mg^{2+} not only are derived from carbonate dissolution, but also other processes, such as cation exchange. Under the mine water group there is a loss of Ca^{2+} and Mg^{2+} relative to HCO_3^-, and there may be other processes leading to the loss of Ca^{2+} and Mg^{2+} and

https://doi.org/10.1021/acsomega.2c04161
ACS Omega 2022, 7, 36387−36402

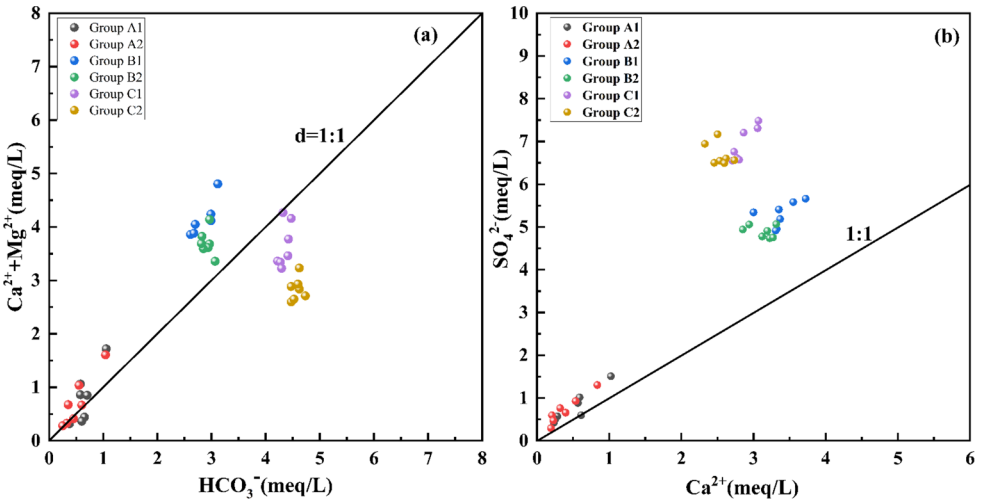

Figure 11. Relationship between the main elements: (a) Ca^{2+} + Mg^{2+}/HCO_3^-, (b) SO_4^{2-}/Ca^{2+}.

possible precipitation of calcite or dolomite and magnesia chlorite.

Gypsum dissolution usually produces equal amounts of Ca^{2+} and SO_4^{2-}, and the SO_4^{2-}/Ca^{2+} concentration ratios of the deionized water group, fissure water, and mine water group all deviated from the gypsum dissolution line (Figure 11b). And all samples are located above the gypsum dissolution line, which indicates a deficit of Ca^{2+} relative to SO_4^{2-}. It also suggests that other sources of SO_4^{2-} may exist. It is possible that SO_4^{2-} originates from the oxidation of pyrite and contains the molar concentration ratio of SO_4^{2-} and Ca^{2+} produced by the neutralization reaction of pyrite (FeS_2) with dolomite, which should be around 2:1 (eq 10).[36]

$$2FeS_2 + 7O_2 + 2CaMg(CO_3)_2 + 2H_2O \rightarrow 2Fe^{2+} + 2Ca^{2+} + 2Mg^{2+} + 4SO_4^{2-} + 4HCO_3^- \quad (10)$$

To further understand the water−rock interaction process of each group, the SI of the main minerals calcite, dolomite, gypsum, and halite were calculated using Phreeqc software and plotted against TDS (Figure 12).

When SI < 0, negative SI values indicate unsaturated conditions and dissolution of minerals, while when SI > 0, positive SI values indicate saturated conditions and precipitation of minerals. Calcite and dolomite have SI values greater than 0 under both fracture water and mine water conditions, which indicates that the minerals are in a saturated state and produce calcite and dolomite precipitation. Gypsum is mostly in an unsaturated state in deionized water. However, it is saturated in mine water and fissure water and may have produced precipitation of gypsum leading to a decrease in Ca^{2+} in the effluent. The SI value of halite was less than 0 under three different water sample conditions, indicating that the halite in the rock sample was in an unsaturated state and the halite produced dissolution, which led to the increase of Na^+ in the effluent water, which was consistent with the results of ion concentration changes in the input and output water in Figure 5.

5.2. Ion Exchange Process. Ion exchange is one of the most important geochemical processes and plays an important role in controlling changes in groundwater chemistry.[37] It can be described by the chlor-alkali index (CAI), which was

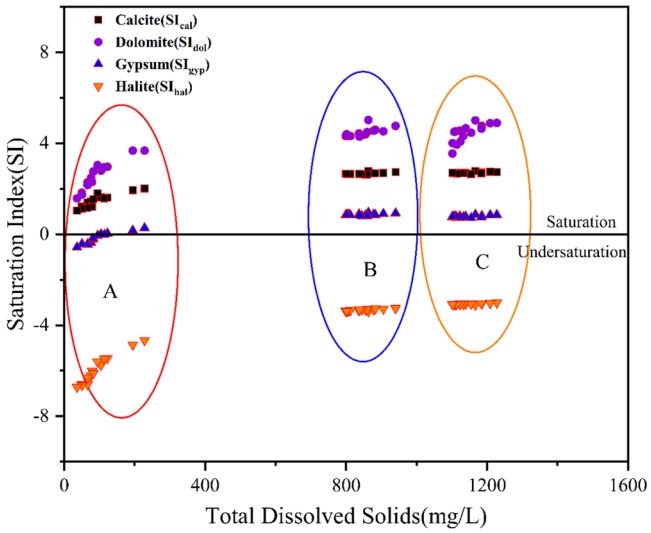

Figure 12. Plot of saturation indices of calcite (SI_{cal}), dolomine (SI_{dol}), gypsum (SI_{gyp}) and halite (SI_{hal}) against TDS.

proposed by Schoeller (1977) to indicate the ion exchange between groundwater and its host environment. According to Schoeller, the CAI value is $[Cl^- - (Na^+ + K^+)]/Cl^-$ (meq/L).

If the CAI is positive, there is a cation exchange reaction (direct exchange) between Na^+ and K^+ in the water and Ca and Mg on the aqueous material. Conversely when the CAI value is negative, there is cation exchange between Ca^{2+} and Mg^{2+} in the water and Na and K on the aqueous material (reverse exchange). In this study, the CAI values ranged from −22.96 to 5.56 (Figure 13a), with negative CAI values for the deionized water group and positive CAI values for the fissure water and mine water groups. It shows that reverse cation exchange occurs in the deionized water environment, and direct cation exchange occurs in the fissure water and mine water environments.

The binary analysis plot of (Na−Cl) versus (Ca + Mg-SO_4-HCO_3) was used to evaluate the cation exchange process.[38,39] These two parameters represent the increase and decrease of Na^+, K^+, Ca^{2+}, and Mg^{2+} in addition to halite, carbonate, and gypsum dissolution. If cation exchange is the dominant process between Ca^{2+}, Mg^{2+}, and Na^+, K^+, these two parameters should be linear with a slope of −1.0.[40] All samples of input and

https://doi.org/10.1021/acsomega.2c04161
ACS Omega 2022, 7, 36387−36402

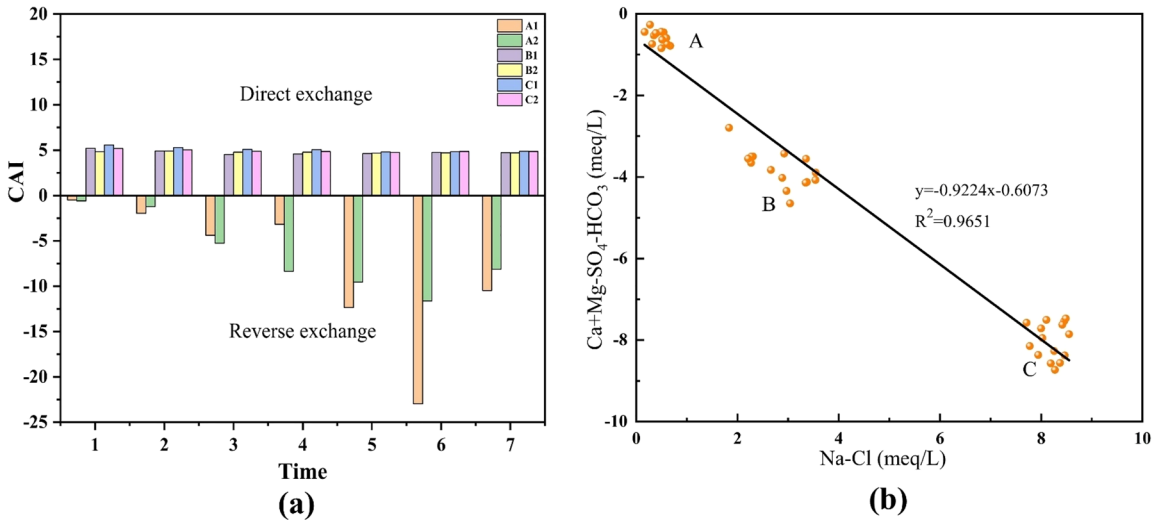

Figure 13. (a) Chloro-alkaline indices of sample, (b) binary diagram Ca + Mg-SO_4-HCO_3 with Na-Cl: A, deionized water group; B, fissure water group; C, mine water group.

output water before and after the experiment were plotted in a binary diagram of (Na−Cl) versus (Ca+Mg-SO_4−HCO_3), as shown in Figure 13b. A straight line with a slope of −0.9224 (R^2 = 0.9651) was fitted to all samples, and all samples were located on both sides of the straight line, which indicated a cation exchange reaction between Na^+, K^+, and Ca^{2+}, Mg^{2+} in the water samples. From the above results, it is shown that the deionized water group is in the unsaturated state for dissolution of Ca^{2+} and Mg^{2+} ions in deionized water due to the low concentration of incoming ions, which leads to the increase of Ca^{2+} and Mg^{2+} ions concentration in deionized water and indirect cation exchange reaction with rock samples. The Na^+ in the mineral is replaced by Ca^{2+} and Mg^{2+} in the water (eq 11). In contrast, fissure water and mine water input water have higher Na^+ concentrations, so direct cation exchange occurs with rock samples. Ca^{2+} and Mg^{2+} in minerals are replaced by Na^+ in water (eq 12).[13]

$$Ca^{2+}(Mg^{2+}) + Na{-}rock \leftrightarrow Ca(Mg){-}rock + 2Na^+ \quad (11)$$

$$2Na^+ + Ca(Mg){-}rock \leftrightarrow Na{-}rock + Ca^{2+}(Mg^{2+}) \quad (12)$$

6. CONCLUSION

In this study, static experimental simulations were performed for two rocks under different water environment conditions of deionized water, fissure water, and mine water. Methods such as multivariate statistics, water chemistry analysis, and rock sample characterization were used to explain the ion change pattern in the input and output water and reveal the type of water−rock interaction during the experiment, and a total of four conclusions were obtained as follows.

1. After the experimental simulation, the input water chemistry type was changed. The deionized water group discharge water chemistry type is 18-A SO_4-Cl-HCO_3-Na-Ca. The fissure water group changed from 39-A type Cl-SO_4-Na-Ca to 42-A type Cl-SO_4-Na. The mine water group changed from 21-A type Cl-SO_4-HCO_3-Na to 42-A type Cl-SO_4-Na. This result is consistent with the water chemistry type of the actual coal mine groundwater reservoir discharge water.

2. There is a difference in the degree of water−rock reaction between two rocks under different ion abundance. The smaller is the ion abundance in water, the more violent is the reaction between water and rock. Under the same conditions, the fine sandstone reacts to a greater extent than the mudstone. As the reaction cycle increases, the water−rock interaction becomes less and less pronounced until balance.

3.After the rocks are soaked with deionized water, the rock mineral composition and surface structure are changed, and there are differences in the dissolution mechanism of fine sandstone and mudstone. The fine sandstone is dissolved from the surface to the inside and around, while the mudstone is further dissolved by creating new pores.

4.The effluent water chemistry was controlled by water−rock reactions and cation exchange during the experiment. The water−rock process consists mainly of halite, silicate, pyrite dissolution, calcite, dolomite, magnesia chlorite, and gypsum precipitation and is accompanied by cation exchange. Mineral dissolution and precipitation are the main factors affecting the ion abundance in the output water.

However, in this study, only conventional ions in water were analyzed, and no heavy metal ions were precipitated from rocks for detection. Therefore, the research on heavy metal precipitation during water−rock interaction needs to be further improved.

AUTHOR INFORMATION

Corresponding Author

Kai Zhang − *School of Chemistry and Environment, China University of Mining and Technology (Beijing), Beijing 100083, China;* orcid.org/0000-0001-7735-7663; Email: zhangkai@cumtb.edu.cn

Authors

Xu Deng − *School of Chemistry and Environment, China University of Mining and Technology (Beijing), Beijing 100083, China*

Ju Gao − *School of Chemistry and Environment, China University of Mining and Technology (Beijing), Beijing 100083, China*

https://doi.org/10.1021/acsomega.2c04161
ACS Omega 2022, 7, 36387−36402

Shuyu Liu − *School of Chemistry and Environment, China University of Mining and Technology (Beijing), Beijing 100083, China*
Fuyao Wang − *School of Chemistry and Environment, China University of Mining and Technology (Beijing), Beijing 100083, China*
Jinglong Han − *School of Chemistry and Environment, China University of Mining and Technology (Beijing), Beijing 100083, China*

Complete contact information is available at: https://pubs.acs.org/10.1021/acsomega.2c04161

Notes

The authors declare no competing financial interest.

■ ACKNOWLEDGMENTS

Thanks to Xingtong Wu for proofreading articles and language assistance during the research process. This work was supported by the Yue Qi Young Scholar Project, China University of Mining & Technology, Beijing (2019QN08), the Talent Introduction Plan of Xinjiang in 2020, Shendong Group Science and Technology Innovation Project (E210100282), the Postgraduate research and innovation ability improvement project, China University of Mining & Technology, Beijing (2021YJSHH19), and the Shendong Group Science and Technology Innovation Project (202016000041).

■ REFERENCES

(1) Dazhao, G. Theory framework and technological system of coal mine underground reservoir. *J. China Coal Soc.* **2015**, *40*, 239−246.
(2) Manyi, F.; Xueyan, L.; Gen, Z.; Qian, L.; Kaiyong, T.; Shuqin, L. Dissussion on water−rock interaction mechanism in undergroud reservoir of Daliuta coal mine. *Coal Sci. Technol. (Beijing, China)* **2020**, 1−8.
(3) Binbin, J.; Shuyu, L.; Jie, R.; Ranfeng, Z.; Mengyuan, C.; Yan, Y.; Kai, Z. Purification effect of coal mine groundwater reservoir on mine water containing organic compounds and heavy metals in different occurrence forms. *Coal Eng.* **2020**, *52*, 122−127.
(4) Anhai, L. New advances in the study of environmental mineralogical materials: Pollution treatment by inorganic minerals-the fourth category of pollution treatment methods. *Front. Earth Sci.* **2005**, 196−205.
(5) Tiantian, W.; Dewu, J.; Jian, Y.; Ji, L.; Qiangmin, W. Assessing mine water quality using a hierarchy fuzzy variable sets method: a case study in the Guojiawan mining area, Shaanxi Province, China. *Environ. Earth Sci.* **2019**, *78*, 8216 DOI: 10.1007/s12665-019-8216-1.
(6) Zhang, K.; Gao, J.; Jiang, B.; Han, J.; Chen, M. Experimental study on the mechanism of water−rock interaction in the coal mine underground reservoir. *J. China Coal Soc.* **2019**, *44*, 3760−3772.
(7) Chunming, H.; Yue, H.; Dengjun, M.; Xing, F. Hydro-geochemistry evolution in Ordovician limestone water induced by mountainous coal mining: A case study from North China. *J. Mt. Sci.-Engl.* **2020**, *17*, 614.
(8) Stradioto, M. R.; Teramoto, E. H.; Chang, H. K. Rock-solute reaction mass balance of water flowing within an aquifer system with geochemical stratification. *Appl. Geochem.* **2020**, *123*, 104784.
(9) He, J. H.; Li, W. P.; Yu, L.; Yang, Z.; Liu, S. L.; Li, L. F. An improved method for determining the position of overlying separated strata in mining. *Eng. Fail. Anal.* **2018**, *83*, 17−29.
(10) Pearce, J. K.; Turner, L.; Pandey, D. Experimental and predicted geochemical shale-water reactions: Roseneath and Murteree shales of the Cooper Basin. *Int. J. Coal Geol.* **2018**, *187*, 30−44.
(11) Ren, J.; Liu, X.; Niu, M.; Yin, Z. Effect of sodium montmorillonite clay on the kinetics of CH4 hydrate - implication for energy recovery. *Chem. Eng.* **2022**, *437*, 135368.
(12) Klunk, M. A.; Dasgupta, S.; Das, M.; Conceicao, R. V.; Siqueira Xavier, S. J.; Chemale, F.; Wander, P. R. Application of geochemical modelling software as a tool to predict the diagenetic reactions between the marine connate water and the salt dome in a petroleum system. *J. S. Am. Earth Sci.* **2021**, *109*, 103272.
(13) Sunkari, E. D.; Abu, M.; Zango, M. S. Geochemical evolution and tracing of groundwater salinization using different ionic ratios, multivariate statistical and geochemical modeling approaches in a typical semi-arid basin. *J. Contam. Hydrol.* **2021**, *236*, 103742.
(14) Sun, J.; Kobayashi, T.; Strosnider, W. H. J.; Wu, P. Stable sulfur and oxygen isotopes as geochemical tracers of sulfate in karst waters. *J. Hydrol.* **2017**, *551*, 245−252.
(15) Haiyan, M. Major ion chemistry of groundwater in the Sangong River Watershed, Northwestern China. *Earth Sci.* **2016**, *75*, 5321 DOI: 10.1007/s12665-016-5321-2.
(16) Loh, A.; Akurugu, B. A.; Manu, E.; Aliou, A. S. Assessment of groundwater quality and the main controls on its hydrochemistry in some Voltaian and basement aquifers, northern Ghana. *Groundwater Sustain. Dev.* **2019**, *10*, 296 DOI: 10.1016/j.gsd.2019.100296.
(17) Zango, M. S.; Sunkari, E. D.; Abu, M.; Lermi, A. Hydro-geochemical controls and human health risk assessment of ground-water fluoride and boron in the semi-arid North East region of Ghana. *J. Geochem. Explor.* **2019**, *207*, 106363.
(18) Belkhiri, L.; Boudoukha, A.; Mouni, L.; Baouz, T. Application of multivariate statistical methods and inverse geochemical modeling for characterization of groundwater — A case study: Ain Azel plain (Algeria). *Geoderma.* **2010**, *159*, 390−398.
(19) Zhu, G. F.; Su, Y. H.; Feng, Q. The hydrochemical characteristics and evolution of groundwater and surface water in the Heihe River Basin, northwest China. *Hydrogeol. J.* **2008**, *16*, 167−182.
(20) Binbin, J.; Ju, G.; Kun, D.; Xu, D.; Kai, Z. Insight into the water−rock interaction process and purification mechanism of mine water in underground reservoir of Daliuta coal mine in China. *Environ. Sci. Pollut. R.* **2022**, 18161 DOI: 10.1007/s11356-021-18161-3.
(21) Duraisamy, K.; Palanisamy, A.; Marghade, D. T.; Subramani, T.; Sunkari, E. D. Appraisal of subsurface hydrogeochemical processes in a geologically heterogeneous semi-arid region of south India based on mass transfer and fuzzy comprehensive modeling. *Geochem. Hlth.* **2020**, 1009.
(22) Lyons, W. B.; Welch, S. A.; Gardner, C. B.; Sharifi, A.; AghaKouchak, A.; Mashkour, M.; Djamali, M.; Matinzadeh, Z.; Palacio, S.; Akhani, H. The hydrogeochemistry of shallow ground-water from Lut Desert, Iran: The hottest place on Earth. *J. Arid Environ.* **2020**, *178*, 1−8.
(23) Qiqing, W.; Wenping, L.; Tao, L.; Xiaoqin, L.; Shiliang, L. Goaf water storage and utilization in arid regions of northwest China: A case study of Shennan coal mine district. *J. Clean. Prod.* **2018**, *202*, 123 DOI: 10.1016/j.jclepro.2018.08.123.
(24) Xiuchang, S.; Zhaoping, M.; Sheng, Y.; Jixing, Z. Simulation of Overburden Deformation failure during Multi-coal Mining in Daliuta Coal Mine. *Met. Mine.* **2015**, 53−57.
(25) Wang, Z.; Dianwu, W.; Kun, L.; Xubo, L.; Yu, C.; Libiao, Y. Hydrochemical Characteristics and Impact Factors in the Middle and Lower Reaches of the Yellow River in the Wet Season. *J. Soil Water Conserv.* **2020**, *27*, 380−386.
(26) Dandan, Z.; Shuxian, F.; Chunyang, H.; Hongwei, Z.; Sirui, Z.; Luyao, Z. Characteristics of organic acids and inorganic components in three-stage fog water in Nanjing. *J. Environ. Sci.* **2020**, *40*, 3342−3351.
(27) Dangyu, S.; Yong, Q.; Junying, Z.; Wenfeng, W.; Chuguang, Z. Washability Characteristics of Hazardous Trace Elements in Coals from Western Region of China. *J. China Univ. Min. Technol.* **2006**, 255−259.
(28) Hao, C.; Huang, Y.; Ma, D.; Fan, X. Hydro-geochemistry evolution in Ordovician limestone water induced by mountainous coal mining: A case study from North China. *J. Mt. Sci.-Engl.* **2020**, *17*, 614−623.

(29) Yidana, S. M.; Banoeng-Yakubo, B.; Aliou, A.; Akabzaa, T. M. Groundwater quality in some Voltaian and Birimian aquifers in northern Ghana-application of mulitvariate statistical methods and geographic information systems. *Hydrol. Sci. J.* **2012**, *57*, 1168−1183.
(30) Bailing, F.; Zhiqi, Z.; Faxiang, T.; Baojian, L.; Zhenghua, T.; Shuang, G.; Lihua, Z. Characteristics of carbonate, evaporite and silicate weathering in Huanghe River basin: A comparison among the upstream, midstream and downstream. *J. Asian Earth Sci.* **2014**, *96*, 5 DOI: 10.1016/j.jseaes.2014.09.005.
(31) Mukherjee, A.; Fryar, A. E. Deeper groundwater chemistry and geochemical modeling of the arsenic affected western Bengal basin, West Bengal, India. *Appl. Geochem.* **2008**, *23*, 863−894.
(32) Jia, H.; Qian, H.; Zheng, L.; Feng, W.; Wang, H.; Gao, Y. Alterations to groundwater chemistry due to modern water transfer for irrigation over decades. *Sci. Total Environ.* **2020**, *717*, 137170.
(33) Houshang, K.; M, R. J. Hydrogeochemistry and quality of groundwater of coastal unconfined aquifer in Amol−Ghaemshahr plain, Mazandaran Province, Northern Iran. *Environ. Earth Sci.* **2014**, *71*, 4767.
(34) Bing, L.; Xunzhen, Z.; Jiajun, J. Numerical simulation of the influence of temperature and sulfate solutionon on the solubility of feldspar. *J. Guangxi Univ., Nat. Sci.* **2012**, *37*, 1008−1012.
(35) Sijing, H.; Keke, H.; Wenli, F.; Hongpeng, T.; Lihong, L.; Xuehua, Z. Mass exchanges among feldspar, kaolinite and Illite and their influences on secondary porosity formation in clastic diagenesis ——A case study on the Upper Paleozoic Ordos Basin and Xujiahe FormationWestern Sichuan Depression. *Geochimica. (Beijing, China)* **2009**, *38*, 498−506.
(36) Zhihong, L.; Guangcai, W.; Xusheng, W.; Li, W.; Zheming, S.; Heike, W.; Shoopala, U.; Collen-Issia, U. Groundwater quality and associated hydrogeochemical processes in Northwest Namibia. *J. Geochem. Explor.* **2018**, *186*, 202.
(37) Blesa, M.; Garcia, G.; del V Hidalgo, M. Geochemistry of groundwater in the alluvial plain of Tucuman province, Argentina. *Hydrogeol. J.* **2001**, *9*, 597.
(38) Ettazarini, S. Processes of water−rock interaction in the Turonian aquifer of Oum Er-Rabia Basin, Morocco. *Environ. Geol.* **2005**, *49*, 293−299.
(39) Rajmohan, N.; Elango, L. Identification and evolution of hydrogeochemical processes in the groundwater environment in an area of the Palar and Cheyyar River Basins, Southern India. *Environ. Geol.* **2004**, *46*, 47.
(40) Fisher, R. S.; Mullican, W. F., III Hydrochemical Evolution of Sodium-Sulfate and Sodium-Chloride Groundwater Beneath the Northern Chihuahuan Desert, Trans-Pecos, Texas, USA. *Hydrogeol. J.* **1997**, *5*, 4−16.

https://doi.org/10.1021/acsomega.2c04161
ACS Omega 2022, 7, 36387−36402